Magnetic Colloidal Particles in Combinatorial Thin-Film Gradients for Magnetic Resonance Imaging and Hyperthermia

Sumera Khizar, Nasir Mahmood Ahmad, Hassan Saleem, Muhammad Asif Hamayun, Sadia Manzoor, Noureddine Lebaz, Abdelhamid Elaissari

Hindawi
Advances in Polymer Technology
Volume 2020, Article ID 7163985, 18 pages
https://doi.org/10.1155/2020/7163985

Research Article

Magnetic Colloidal Particles in Combinatorial Thin-Film Gradients for Magnetic Resonance Imaging and Hyperthermia

Sumera Khizar,[1] Nasir Mahmood Ahmad,[1] Hassan Saleem,[2] Muhammad Asif Hamayun,[3] Sadia Manzoor,[3] Noureddine Lebaz,[4] and Abdelhamid Elaissari[4]

[1]*Polymer Research Lab, School of Chemical and Materials Engineering (SCME), National University of Sciences and Technology (NUST), H-12 Sector, Islamabad 44000, Pakistan*
[2]*Islamabad Diagnostic Center, Islamabad 44000, Pakistan*
[3]*Department of Physics, COMSATS University, Park Road, Islamabad 45550, Pakistan*
[4]*Univ Lyon, University Claude Bernard Lyon-1, CNRS, LAGEPP-UMR 5007, F-69622 Lyon, France*

Correspondence should be addressed to Nasir Mahmood Ahmad; nasir.ahmad@scme.nust.edu.pk

Received 27 March 2020; Revised 20 May 2020; Accepted 4 June 2020; Published 14 July 2020

Guest Editor: Samira Hosseini

A stable oil-in-water (O/W) magnetic emulsion was prepared by the emulsification of organic ferrofluid in an aqueous media, and its theranostic applications were investigated. The synthesis and characterization of the organic ferrofluid were carried out comprising of superparamagnetic maghemite nanoparticles with oleic acid coating stabilized in octane. Both exhibit spherical morphology with a mean size of 6 nm and 200 nm, respectively, as determined by TEM. Thermogravimetric analysis was carried out to determine the chemical composition of the emulsion. The research work described here is novel and elaborates the fabrication of thin-film gradients with 5, 10, 15, and 20 bilayers by layer-by-layer technique using polydimethyl diallyl ammonium chloride (PDAC) and prepared magnetic colloidal particles. The thin-film gradients were characterized for their roughness, morphology, and wettability. The developed gradient films and colloids were explored in magnetic resonance imaging (MRI) and hyperthermia. T1- and T2-weighted images and their corresponding signal intensities were obtained at 1.5 T. A decreasing trend in signal intensities with an increase in nanoparticle concentration in colloids and along the gradient was observed in T2-weighted images. The hyperthermia capability was also evaluated by measuring temperature rise and calculating specific absorption rates (SAR). The SAR of the colloids at 259 kHz, 327 kHz, and 518 kHz were found to be 156 W/g, 255 W/g, and 336 W/g, respectively. The developed magnetic combinatorial thin-film gradients present a significant potential for the future efficient simultaneous diagnostic and therapeutic bioapplications.

1. Introduction

The significant advancement in nanotechnology made possible the production and designing of multifunctional hybrid biomaterials that are highly appropriate for biomedical applications [1]. The development of magnetically engineered colloids is of great interest because of their unique properties and has emerged as promising functional tools for bioapplications for simultaneous diagnostic and therapeutic (theranostic) purposes. Their capability of being manipulated under an external magnetic field provides controllable means of magnetically tagging biomolecules, effective bioseparation, and biosensing, magnetic resonance imaging (MRI) contrast enhancement, and targeted drug delivery [2, 3]. In addition, response to an alternating magnetic field allows the transfer of magnetic energy to the particles in the form of heat, opening the opportunity of being used as an important approach to successful cancer therapy [4].

Among various magnetic nanoparticles, superparamagnetic nanoparticles of single domains of about 5–20 nm as mean diameter particularly magnetite (Fe_3O_4) and maghemite (γ-Fe_2O_3) are promising candidates for biomedical applications due to their biocompatibility [5]. These are widely explored in cancer theranostic bioapplications because of their high magnetic moment, low toxicity, biologically tolerated in a broad range of concentrations, and

synthesis through simplest, economical, and convenient methods using ferric and ferrous salts such as nitrates, chlorides, sulphates, perchlorates, etc. [6]. Recently, magnetic nanoparticles (MNP) coated with biopolymers have gained much attention due to biocompatible, biodegradable, and nontoxic properties of polymers. The organic/inorganic surface coating around iron oxide nanoparticles is essential for biomedical applications. It brings stoichiometric modifications on the surface of nanoparticles, good colloidal stability, and low toxicity in the biological environment and biocompatibility of oxide nanoparticles [7]. Hence, suitable chemical design of magnetic polymer colloids is extremely important in order to make them appealing for magnetic resonance imaging for diagnosis, therapeutic actions of drug delivery, and hyperthermia for combined imaging-guided therapeutics [8].

Depending upon the application, there are several methods to prepare polymeric magnetic nanoparticles among which emulsion technique is the most common and oldest technique [9]. This approach is based on the encapsulation of iron oxide nanoparticles into a biodegradable polymer matrix for improving particle stability and functionalization. In this direction, polyesters such as poly(lactic-co-glycolic acid) (PLGA), polycaprolactone (PCL), polylactic acid (PLA), and polyethylene glycol (PEG) have been reported due to their exceptional characteristics such as biodegradability and biocompatibility [7]. The surface functionalization of the nanoparticles affects the solubility and biodistribution of the colloids inside the body and has a direct influence on imaging capabilities and magnetic behavior of the nanoparticles [10]. Regarding cancer diseases, these colloids are also used as an effective tool for therapy, such as drug delivery and hyperthermia. Furthermore, the employment of magnetic polymer colloids to design multifunctional biothin films by incorporating various materials to obtain molecular-level control presents numerous biomedical applications. The layer-by-layer (LBL) self-assembled multilayer (SAMu) biothin films are not only useful for diagnostics but are also helpful in directing therapeutic agents by focusing on an external magnetic field to the target zone [11]. A broad range of stimuli-responsive thin films have been fabricated and are used as a point-of-care diagnostic devices that can be routinely applied in everyday clinical practice. Thin films of nickel ferrites and chitosan were fabricated by the LBL technique and investigated for their ability to generate an intensity difference using blood as a test liquid; however, T1 and T2 images were not explored in detail [12]. Using the same manual fabrication protocol, thin films were designed, fabricated, and characterized but the magnetic behavior of the films was not tested [13].

In some nanosystems, a combinatorial investigation is best performed in which gradients were incorporated into the thin films for fabricating lab-on-a-chip type films. The development of such combinatorial and high-throughput strategy can eliminate sample preparation steps and permit the development of a disposable chip for a dipstick-like approach toward molecular diagnostics. The combinatorial technique is used not only for identifying new compositions but also for the rapid optimization of the characteristics of the material. The combinatorial approach shows a variation in composition, thickness, and functionality in a single library and allows simultaneous synthesis and screening of large arrays of different materials [14].

Efficient research methods and strategies have been developed for combinatorial fabrication of thin films and their high-throughput characterization. Most frequently, physical and chemical vapor deposition techniques have been applied for the rapid combination of libraries where wide-ranging compositional variation is generated [15].

The current study aims at preparing oil-in-water (O/W) magnetic emulsion by emulsification of organic ferrofluid in an aqueous media. The organic ferrofluid prepared by the coprecipitation method was stabilized in octane. This magnetic fluid was then emulsified in an aqueous solution containing a surfactant to obtain a stable emulsion of magnetic colloidal particles. Multiple techniques were used to characterize the magnetic nanoparticles and the magnetic polymer colloids. In addition, biothin-film gradients were designed and fabricated using magnetic colloidal particles and PDAC solution through the layer-by-layer technique and were characterized to study their morphology/texture and growth. T1- and T2-weighted images of a colloidal suspension of nanoparticles with different iron concentrations were obtained. To the best of our knowledge, combinatorial thin-film gradients were never explored for an in vitro MRI study. Heating response of the prepared magnetic emulsion was also observed for hyperthermia treatment. This research work is the first detailed work dedicated to the fabrication of combinatorial thin-film gradients using the layer-by-layer technique which can be a promising technique in the future for disposable lab-on-chip as a dipstick approach for ultrasensitive molecular imaging of bioanalytes. The technique used for the fabrication of combinatorial thin-film gradients is simple, economical, environmentally friendly, and not time consuming. The developed combinatorial thin-film gradients can further be analyzed as a reservoir for therapeutic drug for in vitro drug release and as a biomimetic multifunctional assembly to develop a point-of-care on chip technology.

2. Materials and Methods

2.1. Materials. $FeCl_2{\cdot}4H_2O$, $FeCl_3{\cdot}6H_2O$, HCl (35%), NH_3 (20%), oleic acid, octane, and polydimethyl diallyl ammonium chloride PDAC (20 wt.% solution) of analytical grade were purchased from Sigma-Aldrich (Germany). Sodium dodecyl sulphate (SDS) used as an anionic surfactant was purchased from Sigma-Aldrich (Germany). Concentrated sulphuric acid (H_2SO_4) (Sigma-Aldrich, 95-98% purity) and potassium dichromate (Scharlau, reagent grade) were used for cleaning the glass substrate. Glass microslides as a substrate for the fabrication of films are from Thermo Fisher Scientific. Ultrapure water was used for the preparation of all solutions. All chemicals/materials were of analytical grades and used as received.

2.2. Synthesis of Magnetic Emulsion

2.2.1. Preparation of Aqueous Ferrofluid. Coprecipitation is a simple and convenient technique to prepare magnetic nanoparticles based on the reduction of metallic elements under

different salt conditions [6]. The ferrofluid synthesis was carried out at 20°C in a thermostatically controlled 500 mL reactor equipped with a mechanical stirring system consisting of a three-branched Teflon anchor. Ferrous and Ferric chlorides were first dissolved in hydrochloric acid (1 M). When the dissolution of the iron salts was completed with the formation of an orange homogeneous solution, the concentrated ammonia solution (20%) was quickly added to the reactor with vigorous stirring at 1000 rpm. The immediate appearance of a black precipitate corresponds to the formation of iron oxide. The coprecipitation reaction is continued in an ammoniac medium for one hour. The pH of the reaction medium was then close to 9.

2.2.2. Preparation of Organic Ferrofluid. The above prepared aqueous ferrofluid was kept under slow stirring in the preparation reactor. The oleic acid was then added directly to the reactor. One hour later, the entire reaction medium was recovered in a beaker. Octane was gradually incorporated into the beaker using a pipette. The mixture was then placed on a magnetic stirring plate for two hours. The iron oxide nanoparticles coated with oleic acid spontaneously pass from the ammoniac phase to the organic phase, which results in very clear phase separation between a clear lower phase (aqueous phase) and an upper phase constituted by the organic ferrofluid.

2.2.3. Preparation of (O/W) Magnetic Emulsion. The first step was to prepare a starting polydisperse emulsion of ferrofluid referred to as "preemulsion." This preemulsion was obtained by gradually incorporating the organic ferrofluid in an aqueous solution containing a surfactant (SDS) with moderate stirring. The prepared magnetic emulsion was highly sheared before performing a magnetic sorting process to obtain narrow size distribution. Octane was removed via evaporation process using rotary evaporation. The final magnetic emulsion was then dispersed in the SDS solution for further characterization and usage.

2.3. Designing Strategy for Fabrication of Combinatorial Thin-Film Gradients. The basic principle of the layer-by-layer technique is the deposition of a substrate such as glass slides in polyelectrolyte and charged colloids solution having opposite charges as presented in Figure 1. Glass slides were first cleaned by overnight dipping in chromic solution (10 wt.% aqueous potassium dichromate: conc. H_2SO_4 50 : 50 *v*/*v*) by which they got negative charges on their surface. In this technique, glass slides were first dipped in positive polyelectrolyte solution for 10 minutes followed by rinsing in ultrapure water twice for five minutes. This results in the first positive layer with the removal of unbound molecules on the glass slide. Then, the glass slides were exposed to the negatively charged solution (solution of prepared magnetic emulsion) again for ten minutes followed by rinsing in ultrapure water twice for five minutes. This results in a single bilayer formation on the substrate that includes one bilayer of polyelectrolyte and magnetic colloids. The number of bilayers deposited is determined by the number of cycles that the substrate undertakes. Following this scheme, combinatorial thin-film gradients were fabricated by varying the exposed surface of the substrate to the solution of polyelectrolyte and magnetic colloids by changing the solution level. Combinatorial thin-film gradients were fabricated having four distinct regions with 5, 10, 15, and 20 bilayers on a glass substrate. The dipping level of the solution is changed after the completion of every 5 bilayers to make gradients in the films.

2.4. Characterization Techniques. The average hydrodynamic diameter (D_h), particle size distribution, and surface charge of the magnetic nanoparticles were determined by Malvern Zetasizer (Nano ZS, Malvern Instruments Limited, U.K). The measurements were carried out in a 1 mM NaCl solution at 25°C. The physical size of the prepared nanoparticles was examined using Transmission Electron Microscopy (TEM, Netherland) with a Philips CM120 microscope at the "Centre Technologique des Microstructures" (CT) at the University of Lyon (Villeurbanne, France). Thermogravimetric analysis of organic ferrofluid and colloids was achieved by the thermogravimetric analyzer (NETZSCH–TG209F1 Iris® ASC, Germany) in the inert atmosphere from room to 600°C temperature at the heating rate of 10°C/min. The magnetic properties of dried magnetic colloids were studied at room temperature by using a vibrating sample magnetometer (Automatic Bench of Magnetic Measurements-ABMM (UK) at the University of Lyon, Villeurbanne, France).

Detailed analysis to determine surface properties of the thin films including film morphology, distribution of colloids, and covered area was observed using low-vacuum analytical scanning electron microscopy (SEM, JEOL JSM 6490LA, Japan) at an accelerating voltage of 20 kV at various magnifications. Morphology and nanostructures of the prepared films were obtained by an atomic force microscope (AFM, Jeol JSPM-5200, Germany) operating in AC or tapping mode, using a commercially available silicon probe. All samples were also imaged using AFM in tapping mode with magnetic force microscopy (MFM) in hover mode under ambient conditions to observe the deposition of bilayers in each section. The contact angle of different sections of the gradient was measured by using drop shape analyzer DSA 25 (KRUSS Advanced 1.8.0.4, Germany) based on the sessile drop technique. To measure the contact angle, a 10-15 μL drop of ultrapure water was placed on the surface of a glass slide using a needle. The angle between the liquid/vapor interface and the solid/liquid interface (i.e., contact angle) was measured by using the ADVANCE software installed in the drop shape analyzer. Film thickness was measured by optical profilometer (NANOVEA PS-50, USA) by moving the probe along the substrate (glass slide) having self-assembly of thin films to acquire the surface height.

2.5. Magnetic Resonance Imaging (MRI) of Magnetic Colloids and Thin-Film Gradients. To study the diagnostic capability of magnetic colloids and their films, MRI was carried out by using a clinical MRI machine (GE SIGNA EXPLORER, USA) of 1.5 Tesla having a FOV of 22 cm and an aperture of 60 cm. Samples were prepared with

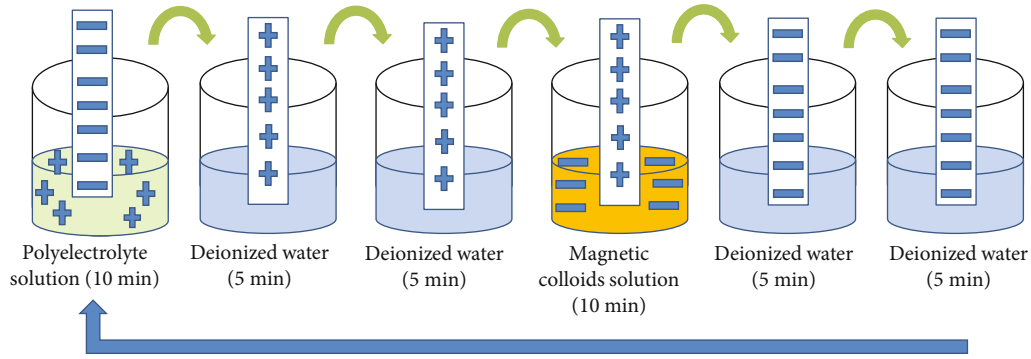

Figure 1: Fabrication of combinatorial thin-film gradients using the layer-by-layer technique.

different concentrations in water in glass vials designated as A0, A1, A2, A3, A4, and A5. T1- and T2-weighted images were obtained with different values of MRI field echo (FE) sequences (TR and TE) to study signal intensity. All samples were placed in the MRI machine on the top of the multichannel body coil. Contrast images were analyzed using host software SV 25 available in MRI machine, and region of interest (ROI) was calculated with the statistical tool K-PACS Workstation (Version 1.5). Water was used as a control to compare the contrast of colloids.

MRI of thin films was also performed using T1 and T2 sequences with different values of MRI field echo (FE) sequences (TR and TE). Glass microslide was immersed in ultrapure water in a custom made polyacrylic cell. Then, the cell is placed inside a magnetic coil to obtain MRI images. The same region of interest was taken in every section of the films having 5, 10, 15, and 20 bilayers, and uncoated region was taken as a reference. The intensity data was measured in Hounsfield units based on the number of pixels contained within the ROI. The relative intensity of each section was measured by taking the mean values of the intensity. All the images were taken in axial mode (along the z-axis) with a slice thickness of 4 mm and a spacing of 1 mm.

2.6. Hyperthermia Study. To study the heating effect of the prepared magnetic colloids, hyperthermia measurement of the prepared magnetic emulsion was done by Nanotheric Magnetherm 1.5 induction unit, operating at different frequencies. The temperature of the field coils was maintained by circulating water at 12°C. A small quantity (1 mL) of the magnetic emulsion was taken in an Eppendorf tube and placed in an insulating cylindrical container under an alternating magnetic field. Temperature rise was noted for a specific time with the "Neoptix optical fiber" temperature sensor. SAR values were calculated by using Equation (1) [16].

$$\mathrm{SAR} = \frac{cM}{m} \cdot \frac{dT}{dt}, \tag{1}$$

where c is the specific heat of the sample, M is the total mass of the sample (in grams), and m is the mass of magnetic nanoparticles (in grams). dT/dt is the initial linear slope of the sample temperature profile obtained by a linear fitting of the experimental data over the short time interval.

3. Results and Discussion

The salient overview of the experimental work is presented in Figure 2 to highlight magnetic colloidal particles and the potential bioapplications of combinatorial thin-film gradients fabricated by using the layer-by-layer technique for MRI analysis and magnetic hyperthermia. MRI analysis showed that the developed film gradients enable us to perform imaging experiments in a single step for disposable lab-on-chip as a dipstick approach for diagnostic applications, and magnetic colloids deposited in film gradients are considered as T2 contrast agents. Hyperthermia measurements of magnetic colloidal particles showed a significant heating effect in an alternating magnetic field to exhibit their suitability for therapeutic applications. The present research has significant potential for advances in polymer technology to design and develop magnetic colloidal particles and their combinatorial thin films for future efficient simultaneous diagnostic and therapeutic bioapplications.

3.1. TEM and Dynamic Light Scattering (DLS) Analysis of Aqueous Ferrofluid and Magnetic Emulsion. The aqueous ferrofluid synthesized by coprecipitation was analyzed by TEM. It was observed that particles were well dispersed with minor aggregation due to the absence of any stabilizer that weakens the magnetic interactions between the particles [17]. No stabilizing agent was used during the synthesis to get superparamagnetic nanoparticles. Agglomeration of particles was due to the attractive forces between the magnetic nanoparticles [18]. Some partial aggregation is probably caused by the preparation of the samples for TEM measurement. The observed clusters may also be attributed to the capillary forces during the drying process of the droplet deposited on the grid before TEM analysis. Results of the TEM analysis in Figure 3(a) showed that the magnetic nanoparticles were spherically shaped and uniformly distributed in size with a mean diameter in number (D_n) of around 6.6 nm and 8 nm as a mean diameter in weight (D_w). The polydispersity index (PDI) was calculated by the analysis of the TEM plate and it was found to be 1.2 (PDI = D_w/D_n). The small size of the particles indicates that the nanoparticles were in the superparamagnetic regime [19]. Figure 3(b) shows the size distribution of aqueous ferrofluid nanoparticles which was carried out using dynamic light scattering

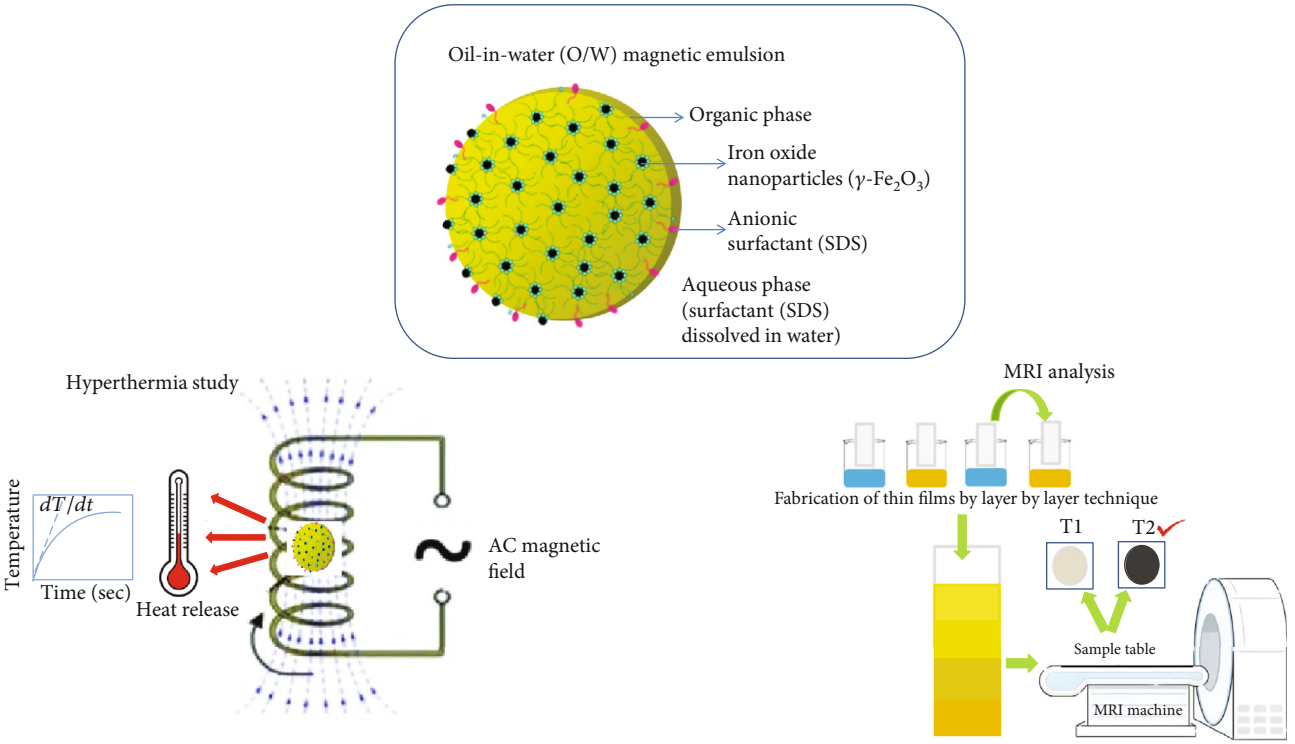

Figure 2: The overview of the magnetic colloidal particle and potential application of combinatorial thin-film gradients fabricated by using the layer-by-layer technique for MRI analysis and colloids for magnetic hyperthermia.

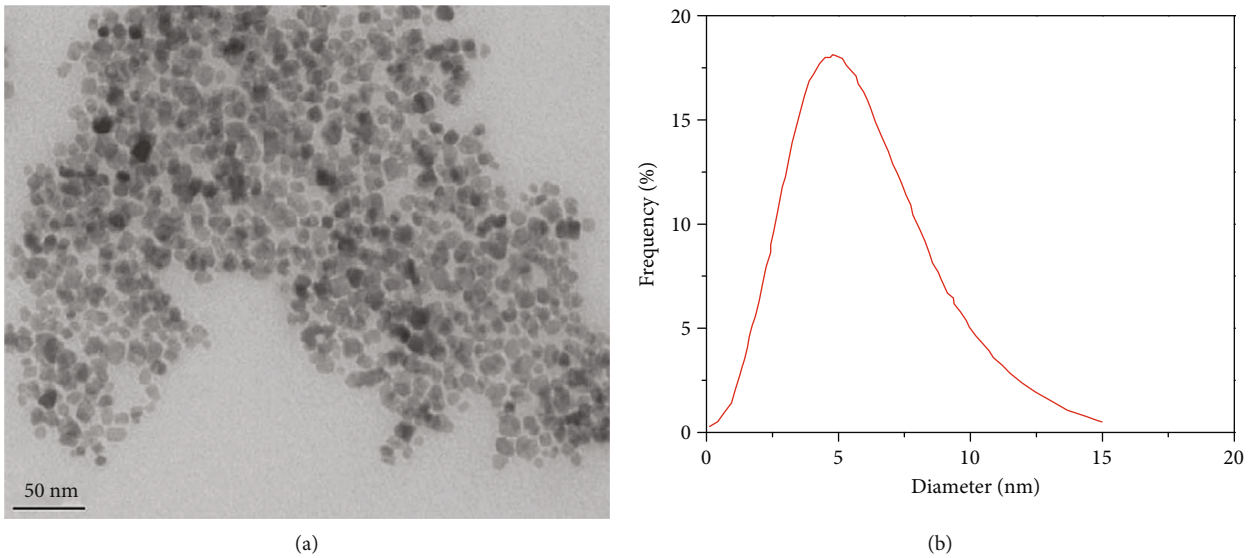

(a) (b)

Figure 3: (a) TEM analysis of the prepared aqueous iron oxide nanoparticles. (b) Dynamic light scattering (DLS) analysis of highly diluted aqueous ferrofluid.

analysis (DLS). The mean hydrodynamic size of the magnetic nanoparticles was found to be around 5 nm which was in agreement with TEM analysis. The narrow size distribution was due to the spherical morphology and negligible magnetic agglomeration [17].

The prepared colloidal particles were also determined by TEM to observe their morphology, structure, and size. TEM images proved the colloidal stability of the particles without aggregation [17]. Figure 4(a) shows the spherical shape of the particles having a smooth surface texture and of nanometric size around 200 nm. The average hydrodynamic particle size was found to be 200 nm with a polydispersity index of 0.023 (Figure 4(b)). The lower value of PDI indicates the monodispersity of the system with an excellent colloidal stability [20]. The zeta potential is the measure of repulsive forces between particles, and its value indicates the colloidal

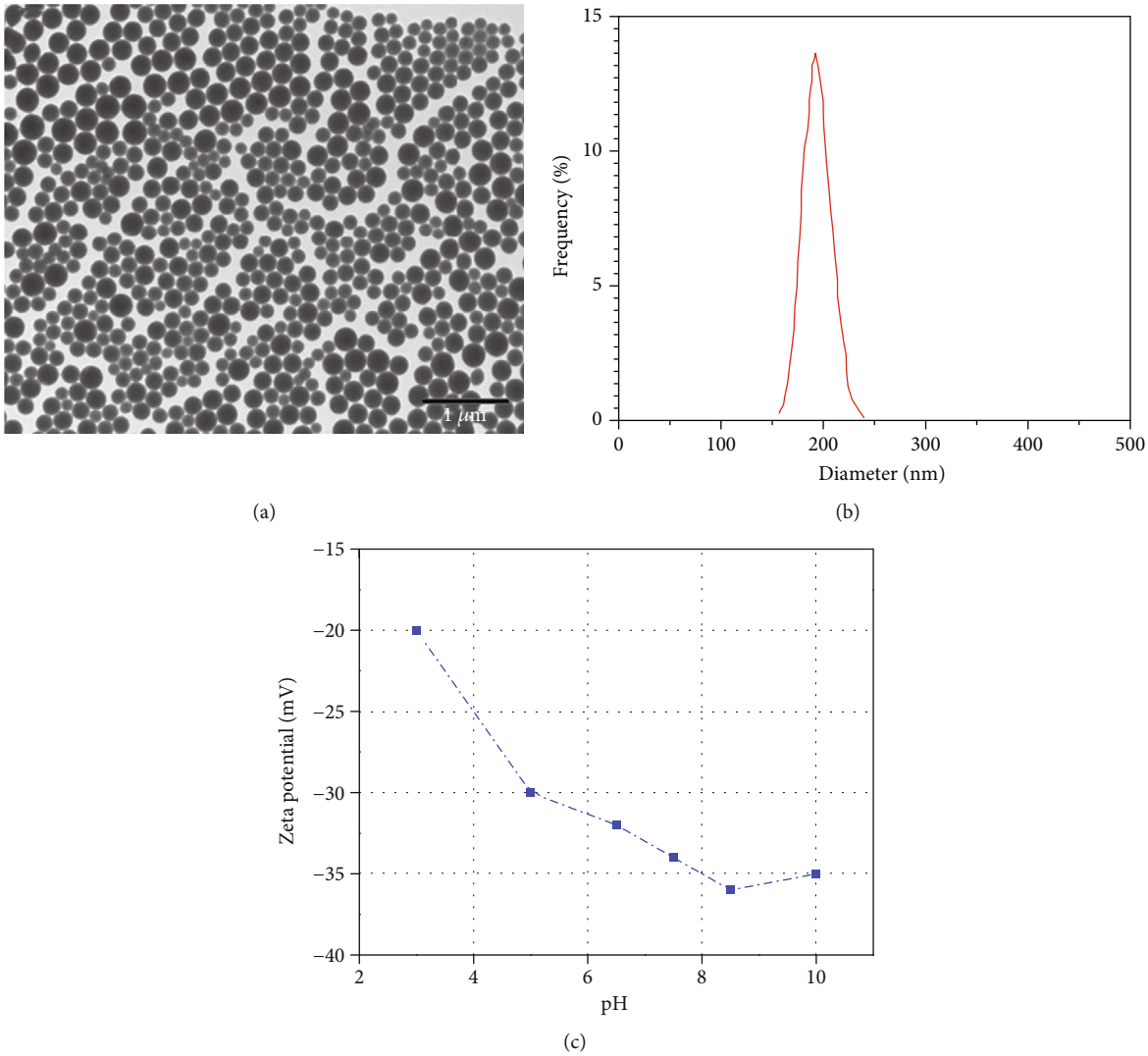

Figure 4: (a) TEM image of the magnetic emulsion. (b) Particle size distribution of the prepared magnetic emulsion via dynamic light scattering technique. (c) Evolution of the zeta potential of the magnetic emulsion as a function of pH.

dispersion stability [21]. Zeta potential of the prepared emulsion as a function of pH was found to be between -20 and -36 mV as shown in Figure 4(c). The observed negative zeta potential was attributed to SDS sulphate groups present on the surface of the magnetic nanoparticles.

3.2. TGA of Organic Ferrofluid and Magnetic Emulsion. For the present study, the objective of thermogravimetric analysis (TGA) was to determine the chemical composition and thermal behavior of the organic ferrofluid and magnetic emulsion based on thermal decomposition. The TGA was used for quantitative analysis to determine both organic and inorganic phases. The TGA profile of pure oleic acid typically exhibited single-step thermal degradation with the maximum rate at around 280°C as several studies reported in the literature [22–24]. In the present work, the TGA was carried out in the range of room temperature to 600°C in an inert atmosphere with a heating rate of 10°C/min. Figure 5 shows the thermal behavior of the organic ferrofluid, illustrating the variations of the residual masses of the samples with the increasing temperature. About 20% of weight loss between 25°C and 550°C is attributed to the degradation of oleic acid in organic ferrofluid [25]. It was also observed that the weight loss is composed of two steps, and this is in good agreement with the reported literature [24]. The first weight loss of about 3% between 25°C and 250°C was due to the loss of oleic acid that acts as an outer layer. The second weight loss of about 17% was attributed to the loss of the oleic acid layer (inner layer) strongly bound to the magnetic nanoparticles because of the covalent bond formation that is related to the affinity between the carboxylic group of oleic acid and ferric and ferrous ions on iron oxide nanoparticles [26, 27]. The amount of maghemite in ferrofluid can be estimated from the residual mass percentages. TGA curve shows that the oleic acid would completely decompose when the temperature reached 550°C. According to mass loss data from the TGA for organic ferrofluid, the maghemite content in the ferrofluid was found to be 80%, showing that the formulation containing 20 wt.% oleic acid with respect to total

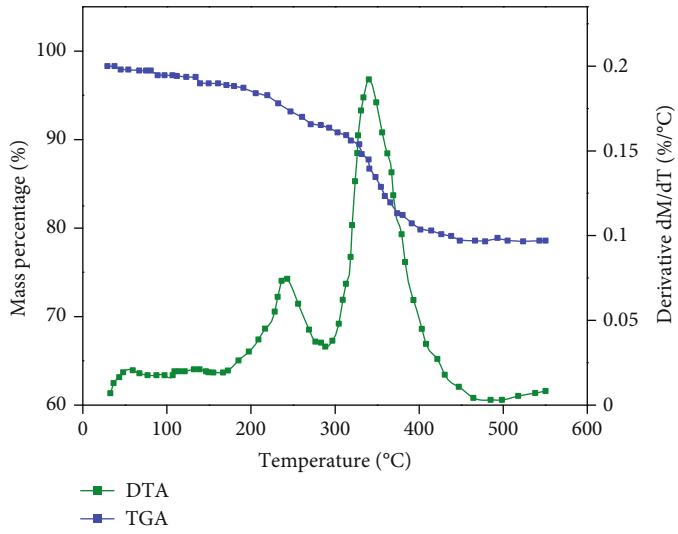

Figure 5: Thermogravimetric analysis (TGA) and differential thermal analysis (DTA) of dried organic ferrofluid.

formulation weight [24, 28, 29]. There were two endotherm peaks observed in DTA (differential thermal analysis) corresponding to the weight loss in two steps in the range of 200°C to 500°C that confirmed the formation of a bilayer of oleic acid on the maghemite surface. The outer layer which was physically adsorbed on the inner layer gets decomposed at a lower temperature while the inner layer that was strongly bonded to the particle surface undergoes decomposition at higher temperature [30]. The second endotherm was observed at around 350°C revealing the complete decomposition of oleic acid.

The iron content in the prepared magnetic emulsion was also determined by thermogravimetric analysis (TGA). This technique consists of measuring the loss of mass of the analyzed sample (in powder form) by thermal degradation of ferrofluid [31]. The crude magnetic emulsion was washed extensively before TGA; this removed all the impurities including the physically adsorbed outer layer of oleic acid. Since oleic acid was used in high excess, therefore, free molecules of oleic acid that formed the outer layer were mainly oriented to the water interface. It resulted in single-step degradation unlike the two-step degradation observed in the case of organic ferrofluid. There was no significantly different thermal change observed as noted in these studies. It is expected that similar trends of thermal degradation of oleic acid took place in the prepared magnetic emulsion. Figure 6 shows that about 25% of the weight loss was due to the degradation of oleic acid in ferrofluid droplets found in the magnetic emulsion [30]. The thermograms for magnetic emulsion show that the loss of mass was gradual. A broad endotherm peak was observed around 350°C that corresponds to the complete degradation of surfactants. Thus, a mass loss using TGA demonstrated that magnetic emulsion was found to be composed of 75% of iron oxides and 25 wt.% oleic acid that remained bound to nanoparticles and could not be washed off [32].

3.3. Magnetization Measurement of Organic Ferrofluid and Emulsion. The saturation magnetization of the ferrofluid is shown in Figure 7. It was determined by extrapolation (magnetic field-H $\rightarrow \infty$) of the line obtained by plotting magnetization – M = f (1/H) and was close to 55 emu/g. This value was close to the theoretically saturated magnetization of maghemite (M_s = 76 emu/g) and reflects the excellent magnetic properties of iron oxide nanoparticles [33]. Differences between experimental and theoretical values were frequently reported in the literature and justified by the existence of defects in the crystal structure or the presence of nonmagnetic compounds incorporated during emulsion formulation [34]. In our case, this difference was mainly attributed to magnetically inactive oleic acid used to prepare organic ferrofluid, which accounts for almost 20% of the total mass of the organic ferrofluid [35]. Considering the composition of the magnetic emulsion, the saturation magnetization reached 40 emu/g, revealing that the superparamagnetic behavior of the magnetic particles was retained after emulsification[33].

3.4. Combinatorial Thin-Film Thickness. The thickness of self-assembled combinatorial thin film gradients depends on the number of bilayers of adsorbed polyelectrolyte and magnetic colloidal particles [36]. Film thickness was measured by optical profilometer, and it was clearly shown in Figure 8 that the thickness varies with the number of bilayers. The thickness increases almost linearly after the deposition of every five bilayers. Less increase in the thickness after the deposition of five bilayers could be due to the substrate effect [37]. The total thickness of films having 5, 10, 15, and 20 bilayers was 50 μm, 82 μm, 142 μm, and 232 μm, respectively. The film thickness increasing with bilayers shows uniform growth of PDAC/magnetic colloids thin films with a distinct interface between coated and uncoated surfaces.

3.5. Scanning Electron Microscopy (SEM) of Combinatorial Thin-Film Gradients. Film morphology, distribution of colloidal particles, and area coverage were determined by SEM at various magnifications. The oppositely charged particles adsorbed onto the substrates have increased with the increase

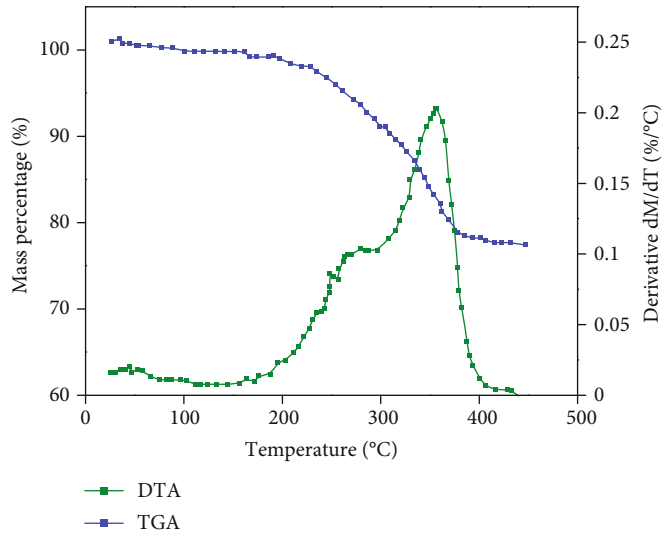

Figure 6: Thermogravimetric analysis (TGA) and differential thermal analysis (DTA) of prepared magnetic emulsion.

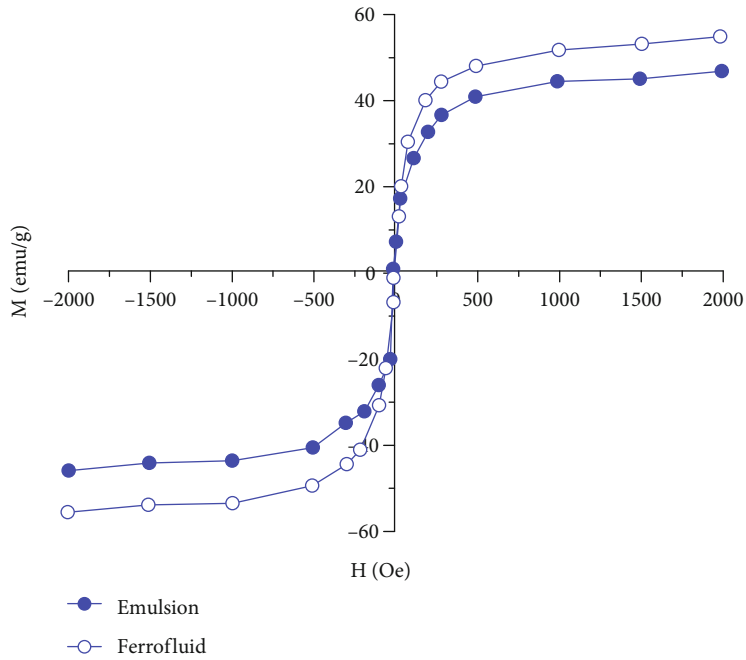

Figure 7: Magnetization versus magnetic field for organic ferrofluid (empty markers) and magnetic emulsion (full markers) under a dried state.

in the number of bilayers. SEM images also revealed agglomeration of particles due to electrostatic attraction between oppositely charged polyelectrolytes showed in Figure 9. The gradient films of PDAC and negatively charged colloids in different bilayer sections undergo charge overcompensation phenomenon that was directly related to layer-by-layer adsorption of particles in successive steps [38]. Increasing the number of washing steps or varying the substrate can lead to a uniform distribution of opposite charges and ensure uniformity in film deposition [39].

Oppositely charged colloids deposited in the first layer served as sites for the second layer. The surface adsorption and agglomeration of magnetic colloidal particles progressively increased with the number of bilayer colloids [40]. In 5 bilayers, much less fractions of glass slide surface area were covered as compared to 10, 15, and 20 bilayers due to substrate effect [37].

Electrostatic interactions between negatively charged magnetic colloidal particles and positively charged PDAC played an important role in the growth of thin films. Thus, one may easily tune the characteristics of the thin films by controlling the colloids concentration on the surface. The magnetic colloidal particles were directly adsorbed on the glass slide without any change in their properties, such as size

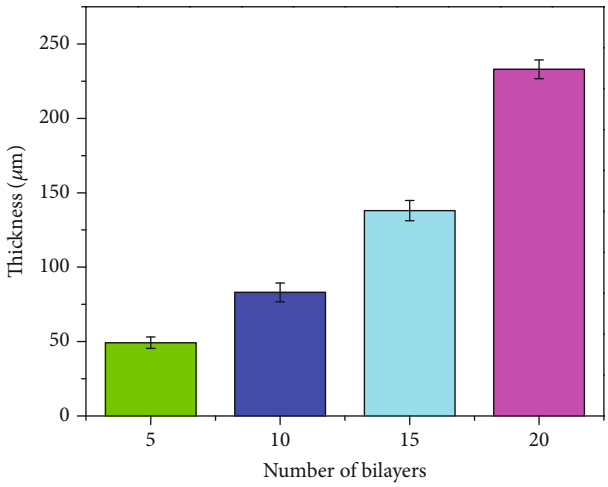

Figure 8: Thickness profile of combinatorial thin-film gradients having 5, 10, 15, and 20 bilayers.

and shape; these are very important for in vitro applications of the films [13].

3.6. Contact Angle of Combinatorial Thin-Film Gradients. Figure 10 shows a decrease in contact angle values with an increase in the number of bilayers that was necessary for T2-weighted MRI contrast agents. The decrease in contact angle with bilayers confirms the phenomenon of charge overcompensation in growing thin films [41] and an increase in hydrophilicity of films that results in greater interaction of water molecules with the fabricated films. There was a regular decrease in contact angle with an increasing number of bilayers. The decreasing trend of contact angle in fabricated gradient films can be attributed to a higher colloidal particles deposition [40]; this is highly important for MRI [13].

3.7. Quantitative Analysis of Topography of Combinatorial Thin-Film Gradients by Atomic Force Microscopy (AFM) and Magnetic Force Microscopy (MFM). AFM and MFM imaging were achieved for each section of the combinatorial thin-film gradient deposited on a glass slide. Figures 11 and 12 shows the AFM and MFM images of thin-film gradients of magnetic colloidal particles. AFM images show the increasing coverage and agglomeration in 3D images as the number of bilayers increases [40]. The gradient trend can be seen from the AFM results in Figure 11 showing that, as the number of bilayers increases, the number of particles deposited also increases along the substrate. It was also observed that the deposition of particles in each section of bilayers (5, 10, 15, and 20) was nonlinear. This type of nonlinear deposition has been observed in the case of the LBL technique [42]. In addition, the distribution of particles on substrates became more uniform with the increase in the number of film bilayers. It is clearly evident that with the increase in the number of bilayers, there is a significant increase in the deposition of magnetic colloidal particles on the surface of the prepared films via a self-assembly process. The number of adsorption sites increased with the number of bilayers indicated the increase in thickness and roughness of the surface [13, 43]. As a consequence, an increase in the number of deposited colloidal particles with the increase in the number of bilayers leads to the increase in surface roughness along the substrate for 5, 10, and 15 bilayers; this is in agreement with the reported literature [12, 13]. But we observed a slightly different behavior of gradient films with 20 bilayers. The surface with 20 bilayers observed to be relatively smoother as compared to surfaces with 5, 10, and 15 bilayers. The root-mean-square values (R_q) of surface roughness were 19.1 nm, 41.2 nm, 47.5 nm, and 34 nm for 5, 10, 15, and 20 bilayers, respectively, whereas average roughness (R_a) values were 12.2 nm, 29.8 nm, 39.2 nm, and 27.3 nm for 5, 10, 15, and 20 bilayers, respectively. The surface roughness of films with 20 bilayers is lower as compared to 5, 10, and 15 bilayers, and that anomaly may be attributed to various factors that affect the resolution of the surface roughness measurement. The AFM system noise effects limit the vertical resolution, and the tip radius effect limits the spatial resolution [44]. Due to these effects, film gradients with 20 bilayers showed a decrease in R_a and R_q values. Tip geometry directly correlates to the roughness value [45]. When the tip is sharp, it obtains an accurate feature of the surface. But as the tip becomes blunt, it cannot approach the bottom of the sample, so it obtains a skewed feature of the surface. In short, as the tip radius increases, the roughness value decreases. In the tapping mode, AFM tip sharpness degraded more than 80%, and its diameter changed significantly as its tip end got damaged progressively during the scans which affect the roughness measurements. The system noise is equally important since when the noise gets mixed into the AFM results; the AFM cannot accurately measure the accurate roughness [46]. The charge on the polyelectrolyte, substrate-PDAC interactions, and substrate dipping time in polyelectrolytes also affected the adsorption behavior in LBL thin films [47]. Agglomeration of colloidal particles was due to the electrostatic interactions between oppositely charged polyelectrolytes on the surface.

MFM images of different sections of bilayers were also carried out to characterize and localize magnetic nanoparticles at the nanoscale as shown in Figure 12. It was clearly evidenced from the MFM images that individual magnetic nanoparticles cannot be detected by MFM because the magnetic field is directly proportional to the diameter of the particles and thus very small. MFM contrast was generated by the interaction between the MFM probe and the magnetic field close to the sample surface. These local nanoscale magnetic interactions cause deflection of the probe which produces a measurable signal monitored for the magnetic imaging of the sample [48]. The phase image contrast represents magnetic force gradient mapping. MFM images of combinatorial gradient films showed that, as the number of bilayers increases, brighter features were higher. An increase in density can be seen through the contrast caused by the magnetic properties of the surface being characterized. Thus, the MFM images showed the magnetic field distribution of a sample on the nanoscale, and no extensive sample preparation is needed. In each section of bilayers, agglomeration of particles in the form of clusters

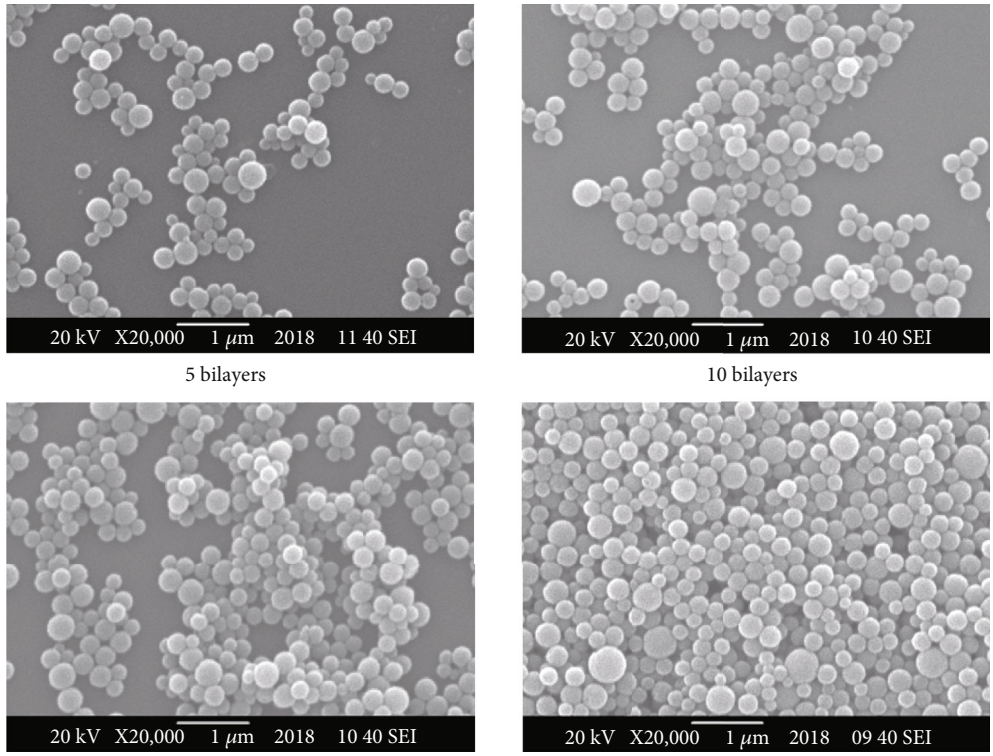

Figure 9: SEM micrographs of combinatorial thin-film gradients of PDAC and magnetic colloidal particles.

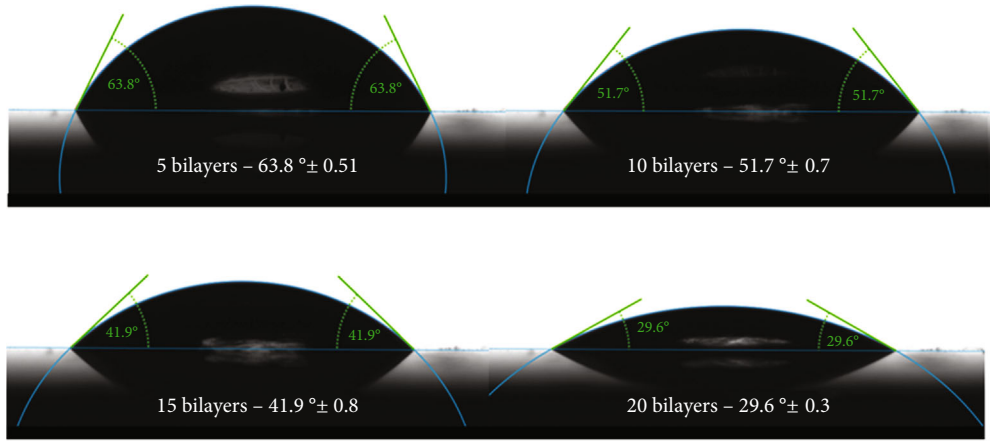

Figure 10: Contact angle measurements of combinatorial thin-film gradients.

was successfully imaged. From the MFM images, one can see the phase shift in terms of degrees resulting from the tip and sample interactions [49]. As the number of adsorbed colloids increases with the number of bilayers, there can be an increase in the interaction between the tip and the substrate that causes the shift in the oscillation of the cantilever. The difference in phase angle between free and interacting cantilever oscillation causes a phase shift that increases with increasing bilayers. The larger the phase shift, the better the magnetic properties of the samples [50]. A negative phase shift over small magnetic domains was observed in MFM images. This was due to attractive interactions between the probe and the magnetic domain. In addition, the magnetically induced phase shift can have both positive and negative regions over a single magnetic domain when the probe-magnetic domain distance is small, rather than being a unidirectional effect [48].

3.8. MRI Analysis of Magnetic Colloids and Combinatorial Thin-Film Gradients. MRI is a very time consuming and expensive diagnostic investigation as compared to other methods such as X-ray and computed tomography (CT). There are no known side effects of MRI scans because it does not involve any kinds of radiations, but it uses magnetism that can distort images of the patients having heart

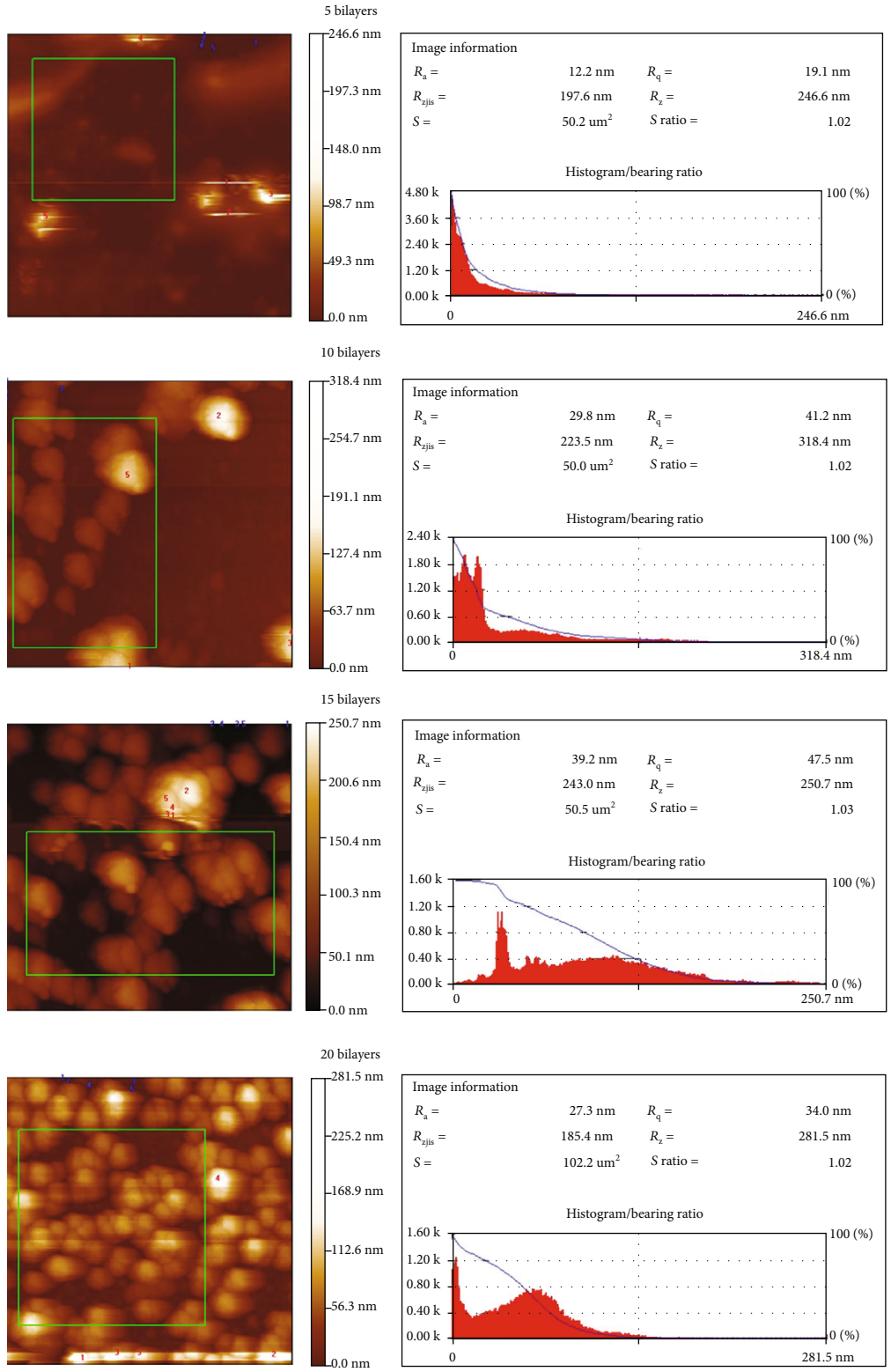

Figure 11: AFM images of combinatorial thin-film gradients of PDAC and prepared magnetic colloidal particles.

pacemakers, metal implants, metal chips, or clips that can interact with the magnet. MRI contrast agents can cause an allergic reaction, flushing sensations, coldness, headache, itching, nausea in patients, and distortion of images obtained by MRI scanners due to the presence of metallic chips, surgical clips, or any other foreign metallic material inside the body. Out of all these side effects, claustrophobia is one of the dominant sensations during MRI scanning in which the patient feels uncomfortable due to the fear of being enclosed or trapped. MRI is also not suitable for patients having

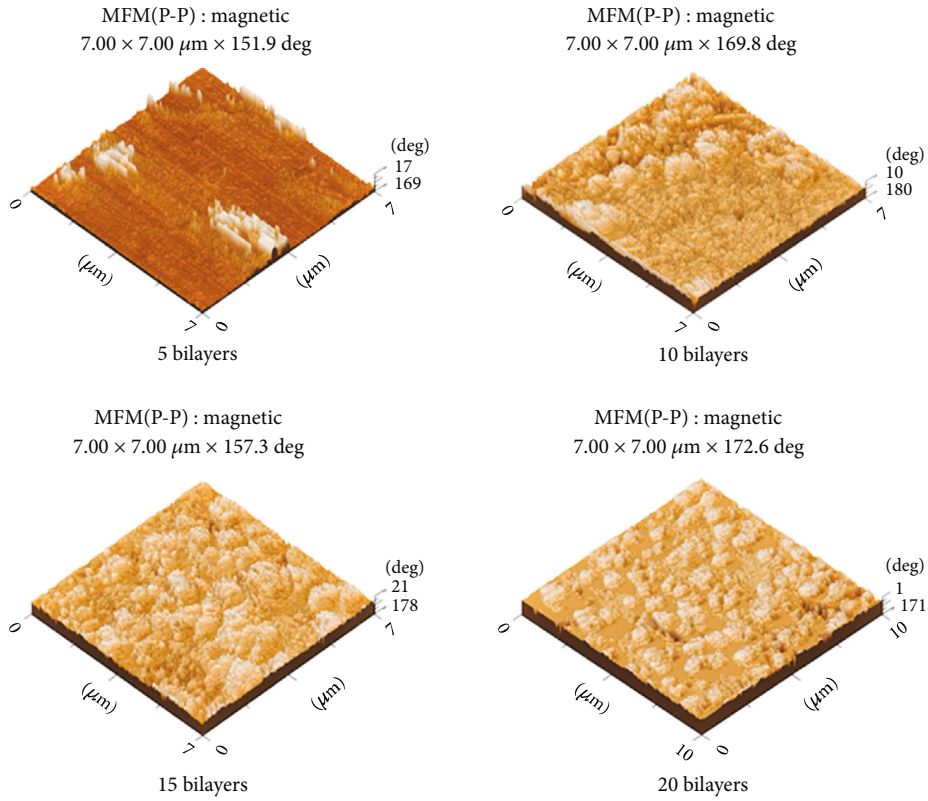

Figure 12: MFM images of combinatorial thin-film gradients of PDAC and prepared magnetic colloidal particles.

asthma, anemia hypotension, and sickle cell disease. Different other methods are used for imaging like X-ray, CT, and positron emission tomography (PET), but MRI is the safest procedure to produce images of the body structures. The main advantage of the present work is the in vitro noninvasiveness diagnosis of biological fluids using combinatorial thin-film gradients. The developed technique lessens the time and expense of the MRI procedure and reduces animal experimentation. The development of such films permits the advancement of the easiest sample application, economic, reproducible, and a disposable chip for dipstick-like approach towards molecular diagnostics.

3.8.1. Effect of Iron Concentration of Colloids on Imaging. Magnetic nanoparticles are considered as T2 contrast agents because they reduced the spin-spin relaxation time [51]. For this purpose, the experimental work carried out to determine the extent to which these particles would enhance the contrast of an MRI image through T1 and T2 sequences. T2 was characterized by spin-spin relaxation time in which the transverse component of the magnetization vector exponentially decayed towards its equilibrium value of zero in MRI. On the other hand, T1 was the spin-lattice relaxation in which longitudinal components of the magnetization vector exponentially recovered to its initial value. Both T1 and T2 are different for different tissues.

MRI characteristics of the prepared O/W emulsion were investigated at various concentrations of iron in the water. Glass vial containing only water was used as a control to compare the contrast capability of the emulsion. These samples were exposed to a magnetic field, a radiofrequency pulse that causes atoms spin and relax after the pulse stops. This relaxation time was detected by the scanners and mathematically converted into an image. The MRI contrast capability of all the samples having different concentrations was analyzed and compared to water. MRI images represent the placement of samples inside the MRI machine. The MRI images were recorded, and equal region of interest (ROI) was drawn manually to obtain average intensity data based on the number of pixels within ROI. Graphs were made using concentrations of iron and acquired ROI intensity. T1-weighted images were obtained by varying TR values (420, 520, 620, 720, and 820 ms) keeping TE fixed at 20 ms, and T2-weighted images were obtained at different TE values (45, 75, 105, 135, and 165 ms) at constant TR 5000 ms.

Figure 13 characterizes the comparison of the average intensity of various samples in the case of T1- and T2-weighted images at TE 75 ms and TR 520 ms. It was observed that all the samples were better T2 contrast agents, as there was no significant effect of concentration on T1 intensity. Also, the T2 negative contrast capability increases with an increase in the concentration of iron in samples that is in good agreement with the reported literature [52, 53]. Compared to water which appeared brighter, T2-weighted images of magnetic colloids appeared to be darker. T2 intensity values of samples indicated their sensitivity as MRI contrast agents.

The T1- and T2-weighted images were obtained through T1 and T2 sequences. As the iron concentration increases in water, signal intensity decreases significantly from higher to

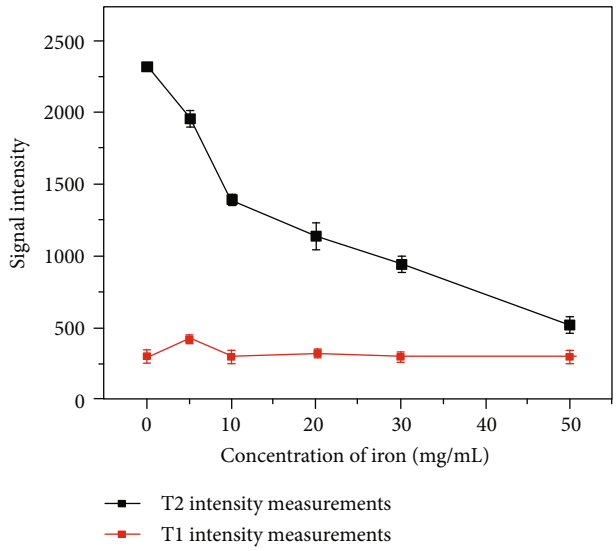

Figure 13: T2 (TE = 75 ms; TR = 5000 ms) and T1 (TE = 20 ms; TR = 520 ms) intensity measurements for various samples. Intensity data is taken as mean intensity within three ROI measurements in terms of intensities of pixels generated from the MRI experiment.

lower values; this is in agreement with the reported values [54–56]. It showed the potential of the prepared emulsion as negative contrast agents. MRI signal intensity varies with TE values. The energy exchanged between protons in water increased with the concentration that resulted in the enhancement of the T2 relaxation rate. An increase in iron concentration creates inhomogeneity in an externally applied field that leads to the dephasing of the magnetic moments and eventually T2 shortening [57]. The lower intensity values compared to water indicated a negative contrast property of these formulations in the case of T2 sequences. The nature of surface coating or functionality on the magnetic nanoparticles also affected the relaxivity of magnetic colloids. It can also be concluded that the emulsification of magnetic nanoparticles in an aqueous phase in this formulation increased the hydrophilicity of particles that allowed greater proximity of water molecules to the nanoparticles, leading to a shortening of T2 relaxation. Hydrophilic and hydrophobic nature of coating affects the degree of hydration and thus their ability to generate contrast in MRI imaging [58]. The surface coating of magnetic particles also prevents the aggregation of particles and thus reduces the interparticle distance that leads to a shortening of the T2 relaxation rate. Relaxivities were strongly affected by particle aggregation [59].

From the results of the signal intensity of T1-weighted images, it was revealed that the concentration of iron did not significantly affect the degree of contrast in T1-weighted images. Thus, the prepared magnetic colloidal particles were considered as T2 contrast agents rather than T1. Surface modification of magnetic nanoparticles influenced the imaging capabilities, hence also affected the T1 relaxivity [58]. It was observed that a sufficient amount of iron is required to generate contrast in MRI and to improve the visibility of internal body structures in MRI [60]. Magnetic resonance imaging contrast agents also induce noticeable relaxation time change in the atoms of body tissues after oral or intravenous administration. The intensity data obtained from MRI images suggest that these formulations could be helpful to develop more effective contrast agents for diagnosis and can be explored for various biomedical applications. Thus, the T2 has strong relaxivity that resulted in a strong variation in T2 signal intensity in the prepared colloids. The mean signal intensity data for all the samples were calculated, and the bar graphs of the mean signal intensity values along with standard deviation values were plotted for each TE sequence (45, 75, 105, 135, and 165 ms) at TR 5000 ms. Signal intensity showed a constant decreasing trend for all the samples at all TE values, which was observed from Figure 14.

3.8.2. MRI Analysis of Combinatorial Thin-Film Gradients. The objective of the present work was also to investigate combinatorial thin-film gradients for their efficacy as contrast imaging agents via MRI to evaluate whether these films were able to generate any contrast. MRI was carried out using a clinical 1.5 T MRI machine. Glass slides having gradients were immersed in a test liquid (ultrapure water) and examined at room temperature. An uncoated region was taken as a reference to compare the difference between the contrasts generated by the gradients. The axial MRI images of thin films were obtained which showed five different regions in combinatorial thin-film gradients (uncoated, 5, 10, 15, and 20 bilayers). The results indicated that magnetic colloids in combinatorial thin films can generate contrast. Signal intensity decreased with the increase in the number of bilayers from 5 to 20. The decrease in signal intensity along the gradient was due to an increase in the number of particles deposited on the slide and a decrease in contact angle that enhances the interaction of water molecules and colloids [13]. An increase in the number of particles adsorbed in thin films along the gradient from 5 to 20 bilayers was evident from SEM results, due to which there is a decrease in MRI intensity count. Due to the hydrophilic nature of the films, it is considered highly efficient to generate contrast in the images formed in MRI scans. Furthermore, functionalization of the surface of magnetic nanoparticles enables their use as multifunctional particles in cancer treatment and multimodality imaging.

Agglomeration of magnetic colloids upon interaction with bioanalytes results in an increase or decrease of MRI intensity, thus showing their potential capability as a contrast agent and forms the base of detection [57]. In the case of combinatorial thin-film gradients, agglomeration was due to the self-assembly of particles rather than interaction with analytes. This study revealed that the combinatorial thin-film gradients of adsorbed magnetic colloids on glass microslides have assisted in decreasing the contrast of the image formed by MRI [52, 53]. This work has significant prospects to enhance and improve the future point-of-care lab-on-chip to develop highly efficient imaging via surface-based MRI of a wide variety of molecules and cells present in the sample of the blood pool such as white blood cells, red blood cells, and platelets. The development of combinatorial gradient thin films eradicated the necessity of injecting magnetic colloids

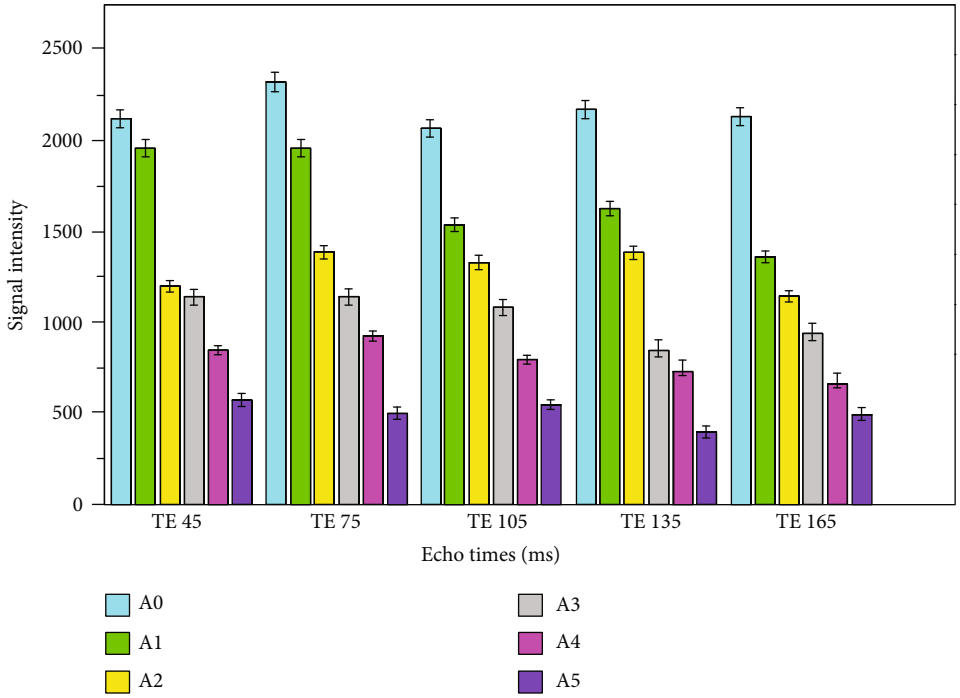

Figure 14: Mean signal intensity graph of different samples for TE 45, 75, 105, 135, and 165 ms and TR = 5000 ms.

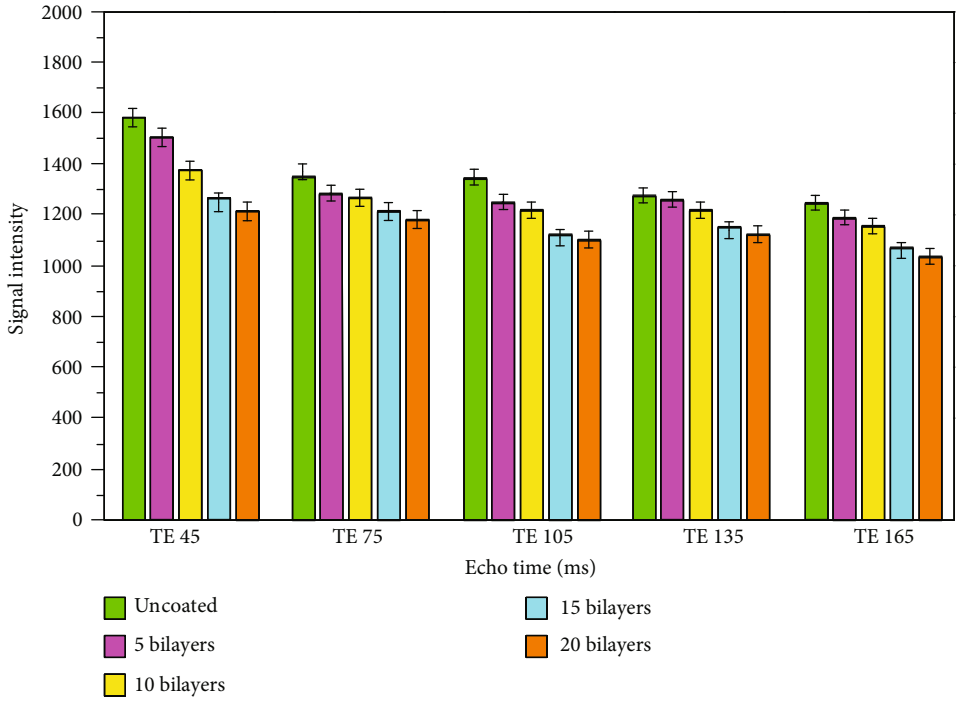

Figure 15: Mean signal intensity graph of combinatorial thin-film gradients for TE 45, 75, 105, 135, and 165 ms and TR = 5000 ms.

into a living body as contrast agents and prevents the association of living organisms in experimentations. Thin films can be fabricated with specific receptors that respond to certain cells which further improve cellular visualization. Difference in contrast in combinatorial thin-film gradients significantly enhances the sensitivity of the films and allows their usage in microfluidic lab-on-chip MRI systems. The mean signal intensity values of uncoated, 5, 10, 15, and 20 bilayer sections in combinatorial gradient thin films were calculated, and the graphs of the mean signal intensity values with standard deviations were constructed against T2 sequence (TE 45, 75, 105, 135, and 165 ms). A persistent decreasing trend in

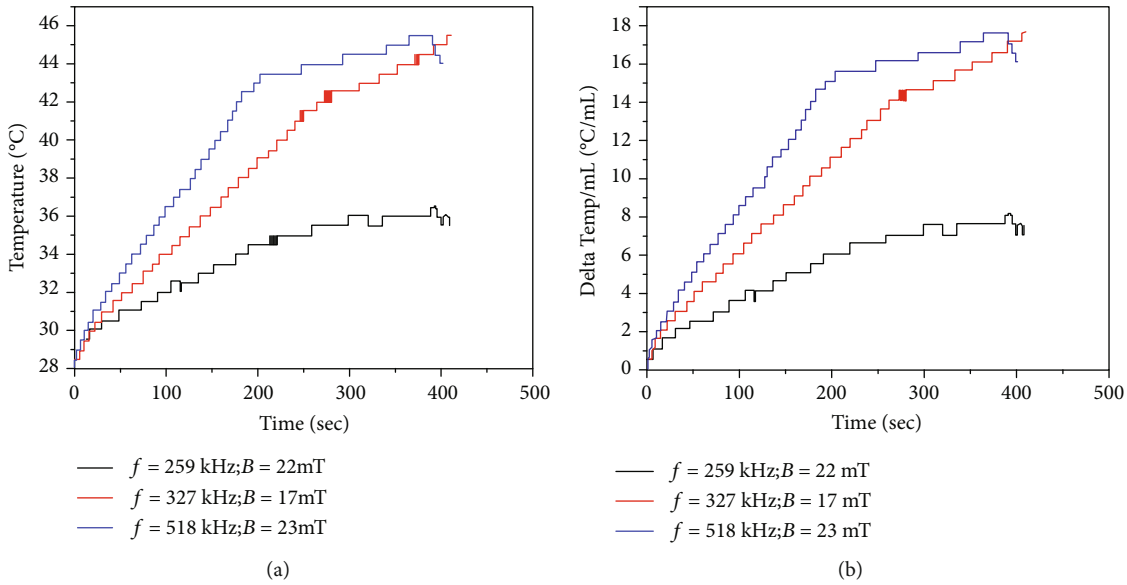

Figure 16: Heating curves of magnetic emulsion taken at different values of AC magnetic field parameters. (a) Hyperthermia measurements of 1 mL of sample. (b) Change in temperature per mL of magnetic emulsion.

intensity was observed at all TE sequences as shown in Figure 15.

3.9. Hyperthermia Measurement of Magnetic Colloidal Particles. This part of the study aimed at evaluating the heating capability of colloidal particles (magnetic emulsion) as hyperthermia mediators. The heating profiles of the sample were estimated and plotted as a function of time, shown in Figures 16(a) and 16(b). The sample was placed in a small vial, inserted in an insulated container to confirm adiabatic condition. Measurements were made at different frequencies (259 kHz, 22 mT; 327 kHz, 17 mT; and 518 kHz, 23 mT) for a specific time (400 sec). The temperature rises with increasing frequency up to a certain limit and then becomes constant [61]. In the present work, maghemite nanoparticles of 6.6 nm as mean size were emulsified in aqueous solution. This mean particle size was less than the critical mean size required for maximum hyperthermia effect (15-18 nm) [62]. The emulsification of organic ferrofluid hinders the heating effect and thus provides better control over the therapeutics. The high heat capacity of the surfactant ensures that the temperature rise was reasonable to avoid overheating, and surface functionalization of nanoparticles regulates the heating performance in hyperthermia. Low content of surfactant over the magnetic nanoparticles had better heating efficacy. There was a maximum temperature rise of 17°C at 518 kHz. As the frequency decreases, there was a different degree of heating observed. Starting from the normal body temperature (37°C), there was a temperature rise of 7°C at 259 kHz, which was suitable for hyperthermia. These results were in concordance with the previously reported values [63]. SAR values at 259 kHz, 327 kHz, and 518 kHz were found to be 156 W/g, 255 W/g, and 336 W/g, respectively. The magnetic emulsion had low SAR values due to the nonmagnetic part in the prepared emulsion and large hydrodynamic size [16].

4. Conclusions

Aqueous and organic ferrofluids consisting of maghemite nanoparticles were prepared by using the coprecipitation method. Single emulsion technique was devised to emulsify these nanoparticles in an aqueous medium. The particle size of nanoparticles and their colloidal particles were determined by TEM and found to be 6 nm and 200 nm, respectively. The iron oxide contents were measured by TGA and found to be 75% in the magnetic emulsion. The saturation magnetization of maghemite nanoparticles was 55 emu/g, which was higher than its colloidal solution due to surface modification. Combinatorial thin-film gradients were also fabricated using a layer-by-layer self-assembly method using PDAC and the prepared magnetic emulsion. The thin films were analyzed by scanning electron microscopy, atomic, and magnetic force microscopy that showed overall an increase in surface coverage with an increase in a number of bilayers. Film thickness was also measured and showed linear deposition of colloidal particles along the substrate. The diagnostic capability of these films and colloids were evaluated by obtaining T1- and T2-weighted images using water as the test liquid. A negative contrast was enhanced as the concentration of iron increases in the samples. Film gradients showed a decreasing trend in intensity with an increase in the number of bilayers. Thus, the developed magnetic combinatorial thin-film gradients from prepared magnetic colloids could be served as a noninvasive medical imaging modality that can be used as a dipstick approach in routine clinical diagnosis. Hyperthermia measurements indicated a significant heating effect of magnetic colloids in alternating magnetic field showed their suitability for therapeutic applications.

Abbreviations

O/W: Oil-in-water

LBL: Layer-by-layer
SAMu: Self-assembled multilayer
PDAC: Polydimethyl diallyl ammonium chloride
SDS: Sodium dodecyl sulphate
MRI: Magnetic resonance imaging
ROI: Region of interest
TE: Echo time
TR: Repetition time
SAR: Specific absorption rate.

Data Availability

The experimental data used to support the findings of this study are available from the corresponding author upon request.

Conflicts of Interest

The authors declare that there are no conflicts of interest regarding the publication of this paper.

Authors' Contributions

Sumera Khizar carried out the experimental work and drafted the manuscript. Nasir M. Ahmad designed and coordinated this research as a principal investigator. Abdelhamid Elaissari assisted in magnetic colloid synthesis, Hassan Saleem carried out MRI studies, and Muhammad Asif Hamayun and Sadia Manzoor participated to perform hyperthermia studies. All the authors read and approved the final manuscript.

Acknowledgments

The authors acknowledge the support of the NUST Research Directorate for support of present work. Sumera Khizar acknowledges the financial support of HEC for the scholarship and the IRSIP program (grant No. 9046) for visiting LAGEPP-UMR, University Claude Bernard Lyon-1, Lyon, France. Dr. Nasir M. Ahmad acknowledges the support of Higher Education Commission (HEC) NRPU (grant No. 3526 and 6020).

References

[1] J. D. Simpson, S. A. Smith, K. J. Thurecht, and G. Such, "Engineered polymeric materials for biological applications: overcoming challenges of the bio-nano interface," *Polymers*, vol. 11, no. 9, article 1441, 2019.

[2] J. Pellico, C. M. Ellis, and J. J. Davis, "Nanoparticle-based paramagnetic contrast agents for magnetic resonance imaging," *Contrast Media & Molecular Imaging*, vol. 2019, article 1845637, pp. 1–13, 2019.

[3] Y. Liu, P. Yin, J. Chen, B. Cui, C. Zhang, and F. Wu, "Conducting polymer-based composite materials for therapeutic implantations: from advanced drug delivery system to minimally invasive electronics," *International Journal of Polymer Science*, vol. 2020, Article ID 5659682, 16 pages, 2020.

[4] S. S. Hayek, "Synthesis and characterization of CeGdZn-ferrite nanoparticles as magnetic hyperthermia application agents," *Advances in Materials Science and Engineering*, vol. 2019, 8 pages, 2019.

[5] T. Guo, M. Lin, J. Huang et al., "The recent advances of magnetic nanoparticles in medicine," *Journal of Nanomaterials*, vol. 2018, Article ID 7805147, 8 pages, 2018.

[6] R. M. Kadhim, E. E. Al-Abodi, and A. F. Al-Alawy, "Synthesis and characterization of magnetic iron oxide nanoparticles by co-precipitation method at different conditions," *Journal of Engineering*, vol. 24, no. 10, 2018.

[7] D. Lombardo, M. A. Kiselev, and M. T. Caccamo, "Smart nanoparticles for drug delivery application: development of versatile nanocarrier platforms in biotechnology and nanomedicine," *Journal of Nanomaterials*, vol. 2019, Article ID 3702518, 26 pages, 2019.

[8] S. Khizar, N. M. Ahmad, N. Ahmed, S. Manzoor, and A. Elaissari, "Encapsulation of doxorubicin in magnetic-polymer hybrid colloidal particles of Eudragit E100 and their hyperthermia and drug release studies," *Polymers for Advanced Technologies*, vol. 31, no. 8, pp. 1732–1743, 2020.

[9] N. Ahmed, N. M. Ahmad, H. Fessi, and A. Elaissari, "In vitro MRI of biodegradable hybrid (iron oxide/polycaprolactone) magnetic nanoparticles prepared via modified double emulsion evaporation mechanism," *Colloids and Surfaces B: Biointerfaces*, vol. 130, pp. 264–271, 2015.

[10] M. K. Lima-Tenório, E. A. G. Pineda, N. M. Ahmad et al., "Aminodextran polymer-functionalized reactive magnetic emulsions for potential theranostic applications," *Colloids and Surfaces B: Biointerfaces*, vol. 145, pp. 373–381, 2016.

[11] J. Xing, Y. Cai, Y. Wang, H. Zheng, and Y. Liu, "Synthesis of polymer assembled mesoporous $CaCO_3$ nanoparticles for molecular targeting and pH-responsive controlled drug release," *Advances in Polymer Technology*, vol. 2020, Article ID 8749238, 8 pages, 2020.

[12] M. A. Hassan, M. Saqib, H. Shaikh, N. M. Ahmad, and A. Elaissari, "Magnetically engineered smart thin films: toward lab-on-chip ultra-sensitive molecular imaging," *Journal of Biomedical Nanotechnology*, vol. 9, no. 3, pp. 467–474, 2013.

[13] A. Ahsan, A. Aziz, M. A. Arshad et al., "Smart magnetically engineering colloids and biothin films for diagnostics applications," *Journal of Colloid Science and Biotechnology*, vol. 2, no. 1, pp. 19–26, 2013.

[14] I. Takeuchi, J. Lauterbach, and M. J. Fasolka, "Combinatorial materials synthesis," *Materials Today*, vol. 8, no. 10, pp. 18–26, 2005.

[15] A. Ludwig, "Discovery of new materials using combinatorial synthesis and high-throughput characterization of thin-film materials libraries combined with computational methods," *NPJ Computational Materials*, vol. 5, no. 1, p. 70, 2019.

[16] F. Reyes-Ortega, A. V. Delgado, E. K. Schneider, B. L. Checa Fernandez, and G. R. Iglesias, "Magnetic nanoparticles coated with a thermosensitive polymer with hyperthermia properties," *Polymers*, vol. 10, no. 1, p. 10, 2018.

[17] M. R. Ghazanfari, S. F. Shams, M. R. Jaafari, and M. Kashefi, "Multi-successive-step pH sensitive procedure: survey of dominant formation mechanism of therapeutic SPIONs," *Ceramics International*, vol. 45, no. 5, pp. 6030–6036, 2019.

[18] M. Circu, A. Nan, G. Borodi, J. Liebscher, and R. Turcu, "Refinement of magnetite nanoparticles by coating with organic stabilizers," *Nanomaterials*, vol. 6, no. 12, p. 228, 2016.

[19] G. Kandasamy, S. Surendran, A. Chakrabarty, S. N. Kale, and D. Maity, "Facile synthesis of novel hydrophilic and

carboxyl-amine functionalized superparamagnetic iron oxide nanoparticles for biomedical applications," *RSC Advances*, vol. 6, no. 102, pp. 99948–99959, 2016.

[20] Y. Tyagi and N. V. S. Madhav, "Smart innovative approach for designing fluvoxamine loaded bio-nanosuspension for the management of depression," *International Journal of Applied Pharmaceutics*, vol. 11, no. 1, p. 191, 2019.

[21] M. H. Hidayat Chai, N. Amir, N. Yahya, and I. M. Saaid, "Characterization and colloidal stability of surface modified zinc oxide nanoparticle," *Journal of Physics: Conference Series*, vol. 1123, article 012007, 2018.

[22] L. A. García-Zapateiro, J. M. Franco, C. Valencia, M. A. Delgado, and C. Gallegos, "Viscous, thermal and tribological characterization of oleic and ricinoleic acids-derived estolides and their blends with vegetable oils," *Journal of Industrial and Engineering Chemistry*, vol. 19, no. 4, pp. 1289–1298, 2013.

[23] M. Seyhan, W. Kucharczyk, U. E. Yarar et al., "Interfacial surfactant competition and its impact on poly(ethylene oxide)/Au and poly(ethylene oxide)/Ag nanocomposite properties," *Nanotechnology, Science and Applications*, vol. 10, pp. 69–77, 2017.

[24] N. V. Jadhav, A. I. Prasad, A. Kumar et al., "Synthesis of oleic acid functionalized Fe_3O_4 magnetic nanoparticles and studying their interaction with tumor cells for potential hyperthermia applications," *Colloids and Surfaces B: Biointerfaces*, vol. 108, pp. 158–168, 2013.

[25] M. M. Rahman, F. Montagne, H. Fessi, and A. Elaissari, "Anisotropic magnetic microparticles from ferrofluid emulsion," *Soft Matter*, vol. 7, no. 4, pp. 1483–1490, 2011.

[26] T. Gong, D. Yang, J. Hu, W. Yang, C. Wang, and J. Q. Lu, "Preparation of monodispersed hybrid nanospheres with high magnetite content from uniform $Fe_{3O}4$ clusters," *Colloids and Surfaces A: Physicochemical and Engineering Aspects*, vol. 339, no. 1-3, pp. 232–239, 2009.

[27] F. Montagne, O. Mondain-Monval, C. Pichot, H. Mozzanega, and A. Elaïssari, "Preparation and characterization of narrow sized (O/W) magnetic emulsion," *Journal of Magnetism and Magnetic Materials*, vol. 250, pp. 302–312, 2002.

[28] J. Mosafer, K. Abnous, M. Tafaghodi, A. Mokhtarzadeh, and M. Ramezani, "In vitro and in vivo evaluation of anti-nucleolin-targeted magnetic PLGA nanoparticles loaded with doxorubicin as a theranostic agent for enhanced targeted cancer imaging and therapy," *European Journal of Pharmaceutics and Biopharmaceutics*, vol. 113, pp. 60–74, 2017.

[29] C. W. Lai, F. W. Low, M. F. Tai, and S. B. Abdul Hamid, "Iron oxide nanoparticles decorated oleic acid for high colloidal stability," *Advances in Polymer Technology*, vol. 37, no. 6, pp. 1712–1721, 2018.

[30] R. P. Araújo-Neto, E. L. Silva-Freitas, J. F. Carvalho et al., "Monodisperse sodium oleate coated magnetite high susceptibility nanoparticles for hyperthermia applications," *Journal of Magnetism and Magnetic Materials*, vol. 364, pp. 72–79, 2014.

[31] R. Y. Hong, B. Feng, X. Cai et al., "Double-miniemulsion preparation of Fe_3O_4/poly(methyl methacrylate) magnetic latex," *Journal of Applied Polymer Science*, vol. 112, no. 1, pp. 89–98, 2009.

[32] J. Mosafer, K. Abnous, M. Tafaghodi, H. Jafarzadeh, and M. Ramezani, "Preparation and characterization of uniform-sized PLGA nanospheres encapsulated with oleic acid-coated magnetic-Fe_3O_4 nanoparticles for simultaneous diagnostic and therapeutic applications," *Colloids and Surfaces A: Physicochemical and Engineering Aspects*, vol. 514, pp. 146–154, 2017.

[33] A. K. Singh, O. N. Srivastava, and K. Singh, "Shape and size-dependent magnetic properties of Fe_3O_4 nanoparticles synthesized using piperidine," *Nanoscale Research Letters*, vol. 12, no. 1, p. 298, 2017.

[34] A. Kumar, P. Kumar, G. Rana, M. S. Yadav, and R. P. Pant, "A study on structural and magnetic properties of NixZn1-xFe$_2$O$_4$ ($0 \le x \le 0.6$) ferrite nanoparticles," *Applied Science Letters*, vol. 1, no. 2, pp. 33–36, 2015.

[35] T. Kim and M. Shima, "Reduced magnetization in magnetic oxide nanoparticles," *Journal of Applied Physics*, vol. 101, no. 9, article 09M516, 2007.

[36] M. Logar, B. Jancar, D. Suvorov, and R. Kostanjšek, "In situ-synthesis of Ag nanoparticles in polyelectrolyte multilayers," *Nanotechnology*, vol. 18, no. 32, article 325601, 2007.

[37] S. S. Shiratori and M. F. Rubner, "pH-dependent thickness behavior of sequentially adsorbed layers of weak polyelectrolytes," *Macromolecules*, vol. 33, no. 11, pp. 4213–4219, 2000.

[38] M. Ulmeanu, M. Zamfirescu, and R. Medianu, "Self-assembly of colloidal particles on different surfaces," *Colloids and Surfaces A: Physicochemical and Engineering Aspects*, vol. 338, no. 1-3, pp. 87–92, 2009.

[39] M. M. de Villiers, D. P. Otto, S. J. Strydom, and Y. M. Lvov, "Introduction to nanocoatings produced by layer-by-layer (LbL) self-assembly," *Advanced Drug Delivery Reviews*, vol. 63, no. 9, pp. 701–715, 2011.

[40] A. G. Osorio, G. B. Machado, M. B. Pereira et al., "Synthesis and characterization of magnetic carbon nanotubes/silsesquioxane nanocomposite thin films," *Applied Surface Science*, vol. 371, pp. 9–15, 2016.

[41] J. B. Schlenoff and S. T. Dubas, "Mechanism of polyelectrolyte multilayer growth: charge overcompensation and distribution," *Macromolecules*, vol. 34, no. 3, pp. 592–598, 2001.

[42] R. K. Iler, "Multilayers of colloidal particles," *Journal of Colloid and Interface Science*, vol. 21, no. 6, pp. 569–594, 1966.

[43] S.-L. Ou, W.-J. Liu, Y.-H. Chang et al., "Structure, magnetic property, surface morphology, and surface energy of $Co_{40}Fe_{40}V_{10}B_{10}$ films on Si(100) substrate," *Applied Sciences*, vol. 10, no. 2, p. 449, 2020.

[44] F. Ruffino and M. G. Grimaldi, "Morphological characteristics of Au films deposited on Ti: a combined SEM-AFM study," *Coatings*, vol. 8, no. 4, p. 121, 2018.

[45] I. Misumi, K. Naoi, K. Sugawara, and S. Gonda, "Profile surface roughness measurement using metrological atomic force microscope and uncertainty evaluation," *Measurement*, vol. 73, pp. 295–303, 2015.

[46] R. Buzio, E. Gnecco, C. Boragno et al., "Self-affine properties of cluster-assembled carbon thin films," *Surface Science*, vol. 444, no. 1-3, pp. L1–L6, 2000.

[47] A. Jung, N. Ha, N. Kim et al., "Multiple transfer of layer-by-layer nanofunctional films by adhesion controls," *ACS Applied Materials & Interfaces*, vol. 11, no. 51, pp. 48476–48486, 2019.

[48] C. S. Neves, P. Quaresma, P. V. Baptista et al., "New insights into the use of magnetic force microscopy to discriminate between magnetic and nonmagnetic nanoparticles," *Nanotechnology*, vol. 21, no. 30, article 305706, 2010.

[49] X. Li, W. Lu, Y. Song et al., "Quantitatively probing the magnetic behavior of individual nanoparticles by an AC field-modulated magnetic force microscopy," *Scientific Reports*, vol. 6, no. 1, article 22467, 2016.

[50] L. Yue, Y. Jin, W. Zhang, and D. J. Sellmyer, "Magnetic force microscopy study of Zr_2Co_{11}-based nanocrystalline materials: effect of Mo addition," *Journal of Nanomaterials*, vol. 2015, 5 pages, 2015.

[51] N. A. Navolokin, S. V. German, A. B. Bucharskaya et al., "Systemic administration of polyelectrolyte microcapsules: where do they accumulate and when? In vivo and ex vivo study," *Nanomaterials*, vol. 8, no. 10, p. 812, 2018.

[52] M. W. Marashdeh, B. Ababneh, O. M. Lemine et al., "The significant effect of size and concentrations of iron oxide nanoparticles on magnetic resonance imaging contrast enhancement," *Results in Physics*, vol. 15, article 102651, 2019.

[53] J. S. Basuki, A. Jacquemin, L. Esser, Y. Li, C. Boyer, and T. P. Davis, "A block copolymer-stabilized co-precipitation approach to magnetic iron oxide nanoparticles for potential use as MRI contrast agents," *Polymer Chemistry*, vol. 5, no. 7, pp. 2611–2620, 2014.

[54] L. M. Ali, P. Marzola, E. Nicolato et al., "Polymer-coated superparamagnetic iron oxide nanoparticles as T_2 contrast agent for MRI and their uptake in liver," *Future Science*, vol. 5, no. 1, article FSO235, 2019.

[55] C. Sanson, O. Diou, J. Thévenot et al., "Doxorubicin loaded magnetic polymersomes: theranostic nanocarriers for MR imaging and magneto-chemotherapy," *ACS Nano*, vol. 5, no. 2, pp. 1122–1140, 2011.

[56] D. M. A. Neto, R. M. Freire, J. Gallo et al., "Rapid sonochemical approach produces functionalized Fe_3O_4 nanoparticles with excellent magnetic, colloidal, and relaxivity properties for MRI application," *The Journal of Physical Chemistry C*, vol. 121, no. 43, pp. 24206–24222, 2017.

[57] Y. Zhang, J. Cheng, and W. Liu, "Characterization and relaxation properties of a series of Monodispersed magnetic nanoparticles," *Sensors*, vol. 19, no. 15, article 3396, 2019.

[58] W. Zhang, L. Liu, H. Chen et al., "Surface impact on nanoparticle-based magnetic resonance imaging contrast agents," *Theranostics*, vol. 8, no. 9, pp. 2521–2548, 2018.

[59] H. T. Ta, Z. Li, Y. Wu et al., "Effects of magnetic field strength and particle aggregation on relaxivity of ultra-small dual contrast iron oxide nanoparticles," *Materials Research Express*, vol. 4, no. 11, article 116105, 2017.

[60] G. Rostoker, M. Laroudie, R. Blanc et al., "Signal-intensity-ratio MRI accurately estimates hepatic iron load in hemodialysis patients," *Heliyon*, vol. 3, no. 1, article e00226, 2017.

[61] N. Griffete, J. Fresnais, A. Espinosa, D. Taverna, C. Wilhelm, and C. Ménager, "Thermal polymerization on the surface of iron oxide nanoparticles mediated by magnetic hyperthermia: implications for multishell grafting and environmental applications," *ACS Applied Nano Materials*, vol. 1, no. 2, pp. 547–555, 2018.

[62] N. Rescignano, Y. González-Alfaro, E. Fantechi et al., "Design, development and characterization of a nanomagnetic system based on iron oxide nanoparticles encapsulated in PLLA-nanospheres," *European Polymer Journal*, vol. 62, pp. 145–154, 2015.

[63] C. Yadel, A. Michel, S. Casale, and J. Fresnais, "Hyperthermia efficiency of magnetic nanoparticles in dense aggregates of cerium oxide/iron oxide nanoparticles," *Applied Sciences*, vol. 8, no. 8, p. 1241, 2018.